

Deep learning-based autofocus method enhances image quality in light-sheet fluorescence microscopy: supplement

CHEN LI,^{1,2} ADELE MOATTI,^{1,2} XUYING ZHANG,^{2,3} H. TROY GHASHGHAEI,^{2,3} AND ALON GREENABUM^{1,2,4,*} 

¹Joint Department of Biomedical Engineering, North Carolina State University and University of North Carolina at Chapel Hill, Raleigh, NC 27695, USA

²Comparative Medicine Institute, North Carolina State University, Raleigh, NC 27695, USA

³Department of Molecular Biomedical Sciences, North Carolina State University, Raleigh, NC 27695, USA

⁴Bioinformatics Research Center, North Carolina State University, Raleigh, NC 27695, USA

*greenbaum@ncsu.edu

This supplement published with The Optical Society on 22 July 2021 by The Authors under the terms of the [Creative Commons Attribution 4.0 License](https://creativecommons.org/licenses/by/4.0/) in the format provided by the authors and unedited. Further distribution of this work must maintain attribution to the author(s) and the published article's title, journal citation, and DOI.

Supplement DOI: <https://doi.org/10.6084/m9.figshare.14924751>

Parent Article DOI: <https://doi.org/10.1364/BOE.427099>

Deep Learning Based Autofocus Method Enhances Image Quality in Light-Sheet Fluorescence Microscopy

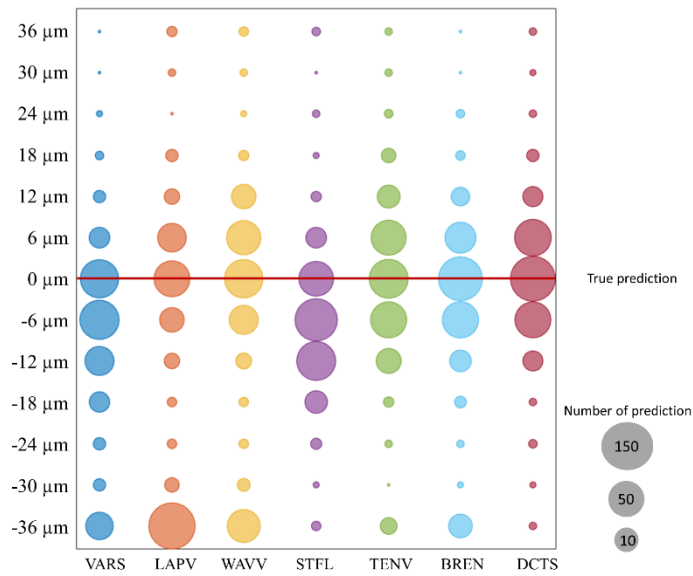


Fig. S1. Comparison between traditional autofocus quality measures. The bubble chart shows the prediction of various methods when a full stack (13 images) is provided as an input. In all the cases (~420) the true prediction is at 0 μm. From left to right, the methods are image variance (VARS), Variance of Laplacian (LAPV), Variance of Wavelet coefficients (WAVV), Steerable filters (STFL), Tenengrad variance (TENV), Brenner's measure (BREN), Shannon entropy of the normalized discrete cosine transform (DCTS). DCTS shows the best performance among the tested methods.

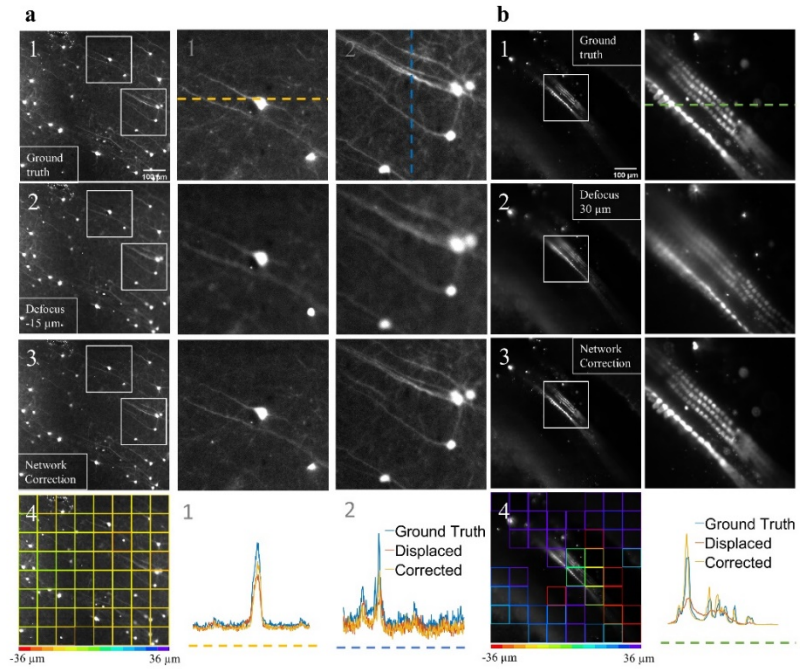


Fig. S2. Real-time perturbation experiments in light-sheet fluorescence microscopy. (a1 and b1) The in-focus ($\Delta z = 0$) images of neurons and hair cells, respectively. (a2 and b2) Images that show the same field of view as in a1 and b1 after the objective lens was displaced by $-15 \mu\text{m}$ and $30 \mu\text{m}$, respectively. (a3 and b3) Images of the same field of view after the objective was moved according to the network defocus prediction as shown in a4 and b4. The improved image quality in a3 and b3 indicates that the network can estimate the defocus level and adjust the detection focal plane to improve image quality. In a and b, the white boxes mark the location of the zoom in images, and the line profiles in a4 and b4 represent image intensities along the dashed lines in a and b.

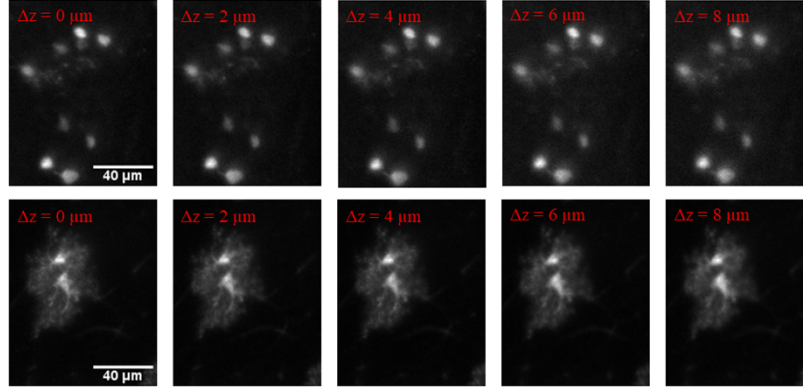


Fig. S3. Changes in image quality over small defocus distances. Representative examples of defocused images with small defocus (Δz) values. Changes in image quality are observed by eye starting from Δz distance of $6 \mu m$.

Table S1. Performance comparison between DNN and DCTS on 3×3 tiles with various conditions.

Condition	Absolute distance between predicted and actual position
DNN (with certainty)	3.8976 μm
DNN (without certainty)	4.3048 μm
DCTS (9 tiles and average)	5.1857 μm
DCTS (9 tiles and average with certainty)	4.7599 μm
DCTS (one tile 384×384 pixels)	4.1857 μm

Note: all 420 test images are randomly cropped from the test dataset (42 stacks), the size of the test image is 384×384 (pixels), which is exactly 3×3 tiles. In general, DNN performs better when tiles with low certainty are excluded, and DCTS performs better when it is provided the entire 384×384 pixels as input. The certainty values for the DCTS were provided from the DNN.